Available online at www.sciencedirect.com
ScienceDirect
Journal of Power Sources 174 (2007) 373–379
JOURNAL OF POWER SOURCES
www.elsevier.com/locate/jpowsour

Low-temperature study of lithium-ion cells using a Li_ySn micro-reference electrode

Andrew N. Jansen *, Dennis W. Dees, Daniel P. Abraham, Khalil Amine, Gary L. Henriksen

Electrochemical Technology Program, Argonne National Laboratory, Argonne, IL 60439-4837, USA

Available online 3 July 2007

Abstract

Lithium-ion batteries are considered to be the next battery system for hybrid electric vehicles (HEVs) due to their high power density. However, their power is severely limited at −30 °C and the concern exists that lithium metal could plate on the negative electrode during regen (charge) pulses. The goal of this work is to determine the reason for this poor low-temperature performance using an *in situ* Li_ySn micro reference electrode (RE) over a wide temperature range of 30 °C to −30 °C. A variety of negative and positive electrode materials with unique morphologies was used in this work to help elucidate the dominant low-temperature mechanism. In this work, it was observed that the potential of graphite negative electrodes does dip below lithium potentials not only during charge pulses, but also under normal charging if the cell cutoff voltage is not reduced from its room-temperature setting of 4.1 V, whereas hard carbon electrodes do not because they operate further from lithium potential. The most surprising finding from this work was that a second impedance mechanism dominates below 0 °C that affects the positive and negative electrodes almost equally. This suggests that the responsible phenomenon is independent of the active material and is most likely a pure electrolyte-interface effect.

Keywords: Lithium-ion; Battery; Low temperature; Reference electrode; Lithium plating; Surface area; $Li_4Ti_5O_{12}$

1. Introduction

Lithium-ion batteries have received much interest for use in hybrid electric vehicles (HEVs). While lithium-ion batteries have abundant power at room temperature, their power is poor at the low temperatures that HEVs will experience in normal use. The concern also exists that lithium metal will plate on the negative electrode during charge pulses (regen). The U.S. Department of Energy's (DOE's) Advanced Technology Development (ATD) program has been tasked by DOE's FreedomCAR and Vehicles Office to understand and solve these limitations. A low temperature goal was set requiring that a battery rated at 25 kW must be able to provide three 2-s discharge pulses of 5 kW with 10-s rests in between at −30 °C. These pulses would simulate starting a cold engine. More on the HEV battery requirements and testing protocols can be found in [1].

The work presented here reflects the low-temperature performance of laboratory sized cells evaluated under conditions relevant to an HEV. The goal of this work is to determine the influence that active material choice has on impedance, capacity utilization, and potential at low temperature with a particular emphasis on graphite morphology.

Many researchers have attempted to improve the low-temperature performance of lithium-ion batteries by developing electrolytes with high ionic conductivities at low temperature [2–5]. Extensive work on developing new low-temperature electrolyte formulations was done in the aerospace industry [6–8] with an emphasis on energy utilization. However, it was observed early on in our work with electrodes designed for high-power applications, such as in HEV batteries, that the impedance rose over an order of magnitude upon lowering the temperature from 30 °C to −30 °C. Such a large impedance rise could not be explained by electrolyte conductivity effects alone. Clearly, another mechanism was at work.

An *in situ* technique was needed that could elucidate the reason for the poor low-temperature performance. The ideal choice is to incorporate a micro-reference electrode between the positive and negative electrodes. The placement of the reference electrode can have a direct impact on the accuracy of the impedance results. Reference electrodes positioned in the electrolyte pool outside of the electrode area will reflect the potential field of the electrode nearest it if the electrodes are

* Corresponding author. Tel.: +1 630 252 4956; fax: +1 630 972 4461.
E-mail address: jansen@cmt.anl.gov (A.N. Jansen).

0378-7753/$ – see front matter © 2007 Elsevier B.V. All rights reserved.
doi:10.1016/j.jpowsour.2007.06.235

Table 1
Physical properties of active materials used in this study

Active material	Particle size D50/D90, μm	Surface area, m^2/g (BET)	Comments
GMCF Petoca Ltd.	13/35	2.8	MELBLON milled carbon fiber, meso-phase pitch
MCMB-25–28 Osaka gas chemicals	22.4/37.0	0.85	Spherical graphite beads
GDR-AA-3-3 Mitsui Mining Co.	16.2/21.1	3.2	Carbon-coated natural graphite
MAG-10 Hitachi Chemical Co.	10.1/21.4	5.2	Synthetic graphite, Gen2 negative
MCMB-10–28 Osaka gas chemicals	11.82/NA	2.01	Synthetic graphite, Gen3 negative
LINILITE CA1505N Fuji chemical	10.3/17.1	0.78	Gen2 positive $LiNi_{0.85}Co_{0.1}Al_{0.05}O_2$
L333 Seimi Chemical	12.2/NA	0.41	Gen3 positive $Li[Li_{0.1}Ni_{0.3}Co_{0.3}Mn_{0.3}]O_2$

offset by as little as a tenth of a millimeter [9]. Hence the need exists to place the RE in between the electrodes. However, the dimensions of lithium-ion cells make the inclusion of an ideal RE quite difficult; a typical separator is less than 30-μm thick.

Compromises have to be made. Thin lithium strips were originally used in between two separators with limited success. The main problems were (1) difficulty in producing and handling lithium strips with diameters near 30 μm, and (2) no effective means of masking the lithium in the regions outside of the electrode perimeter. Micro REs were then made by plating lithium onto 25-μm-diameter gold-plated wires in which exterior regions of the wire were masked with a polyurethane coating. These REs were more successful, but occasional shorts would develop due to lithium dendrites growing in the separator pores during lithium deposition. Efforts were then directed to develop micro reference electrodes along the lines of Johnson and Dees [10]. These REs are based on Li_ySn formation on an inert wire substrate, which avoids the issue of lithium dendrites. While reliable impedance data can be produced from Li_ySn REs, determining the true potential of each electrode is not straightforward because of the multiple voltage plateaus of Li_ySn.

2. Experimental approach

In this work, the electrochemical processes taking place in the negative and positive electrodes were investigated using an *in situ* micro-RE in cell hardware that was developed earlier [11]. The micro-RE consists of a 1-μm-thick tin coating on a 25-μm-diameter copper wire that is coated with an insulating polyurethane coating. A 1-cm length of the polyurethane coating is removed prior to use to expose the tin surface. Cells were assembled with the micro-RE placed between separator layers and then charged with lithium from either electrode to form Li_ySn. In cells that used graphite as the negative electrode, the Sn was easily lithiated by shorting the Sn reference electrode to the fully charged graphite via 100-kΩ, 10-kΩ, 100-Ω, and 0-Ω resistors sequentially. A sequence of resistors was used with the expectation that the Sn would lithiate gradually and thus minimize stress effects due to volume expansion. For cells that used non-graphitic electrodes, the Sn RE was charged from the positive electrode via a potentiostat.

A variety of negative electrodes was used in this study and includes: MAG-10 (referred to as "Gen2 negative" in this study), GMCF, MCMB-25, GDR-AA-3-3, MCMB-10 (referred to as "Gen3 negative"), hard carbon, and $Li_4Ti_5O_{12}$. Two cathode materials were used as the positive electrode in this study: $LiNi_{0.85}Co_{0.1}Al_{0.05}O_2$ (referred to as "Gen2 positive") and $Li[Li_{0.1}Ni_{0.3}Co_{0.3}Mn_{0.3}]O_2$ (referred to as "Gen3 positive"). The physical properties and makers of these active materials are listed in Table 1. Electrodes were made with the materials in Table 1 by battery manufacturers Quallion LLC (Sylmar, CA) and/or Enerland Co., Ltd. (Gyeonggi-Do, Korea). Electrodes were also made in-house with hard carbon and with $Li_4Ti_5O_{12}$.

The electrodes were made with 8 wt% PVDF binders (Kureha KF 9130 was used for all negative electrodes except Gen3-Enerland, which used Kureha PVDF 1100; Kureha KF 1120 was used in Gen2 and Gen3-Quallion positive electrodes; and Kureha KF 7208 was used in the Gen3-Enerland positive electrode). Carbon additive was added to the positive electrodes to improve their electronic conductivity (4 wt% Timcal SFG-6 graphite plus 4 wt% Chevron C-55 acetylene black was used in the Gen2 positive; 8 wt% Tokai TokaBlack #5500 carbon black was used in the Gen3 positive from Quallion; and 8 wt% Timcal Super P™ carbon black was used in the Gen3 positive from Enerland).

The electrolyte used in this study was 1.2 M $LiPF_6$ in a mixture of ethylene carbonate and ethyl methyl carbonate (EC/EMC, 3:7 by wt), which remains liquid below −40 °C. Precipitates do form at −60 °C in this electrolyte that do not re-dissolve until the temperature is raised above −10 °C. This electrolyte was developed earlier in the ATD program [2] and is referred to as "Gen2 electrolyte". Electrode areas of 32 cm^2 were used in custom-designed stainless steel fixtures as shown in Fig. 1. An oversized polyethylene gasket with a 3-cm margin around the lab cell was used between the positive and negative fixture plates to prevent complications due to mois-

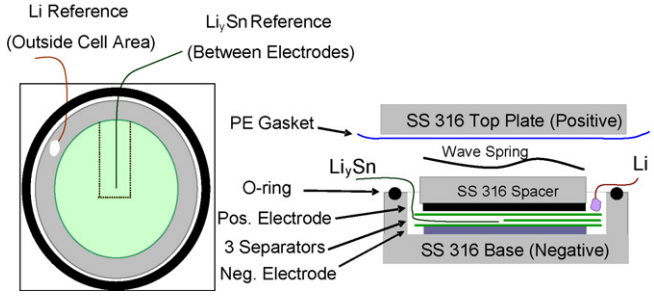

Fig. 1. Test fixture and cell configuration used in this study. Hardware was bolted together with insulated washers.

ture condensation on the lab cell when the temperature is increased above the relative dew point. Celgard 2325, which is a trilayer (polypropylene/polyethylene/polypropylene) microporous membrane, was used as the separator. Cells that were made with a Li_ySn reference electrode used three layers of separator with a notch cut from the middle separator layer to accommodate the thickness of the reference electrode wire.

Various combinations of electrodes were used in this study to make lithium ion cells that had negative to positive capacity ratios that ranged from 1.1 to 1.5. Two constant-current formation cycles were performed on each cell at room temperature that consisted of charge and discharge at a C/5 rate between 3.0 and 4.1 V (4.0 V for Gen3 electrodes from Enerland). Upon completion of the formation cycle, 8 cycles were performed in total: 2 cycles at 0.3 mA/cm^2, 3 cycles at 0.6 mA/cm^2, and 3 cycles at 1.0 mA/cm^2. A plot was then made of the discharge capacity versus discharge time in hours and the C/1 capacity was determined via interpolation/extrapolation of this plot at the 1 h mark. One hybrid pulse power characterization (HPPC) test [1] was then performed on each cell at a 5C current rate (2.5C rate was used at −30 °C due to high impedance). The temperature was then changed and this 9-cycle sequence was repeated at each temperature. The 5C pulse current was based on the C/1 capacity determined at each temperature (see Fig. 2), not the C/1 capacity at 30 °C. The voltage window was widened to 1.0 and 4.6 V during the HPPC pulses at low temperature to guarantee a complete data set. Constant voltage charges were used with current limited to the selected discharge current (i.e., 0.3, 0.6, and 1.0 mA/cm^2).

The temperatures used in this study followed the sequence 30 °C, 0 °C, −30 °C, 15 °C, −10 °C, −20 °C, and then 30 °C to check for cell degradation. Capacity and impedance values differed by only a few percent between the initial and final tests at 30 °C. Charges were performed at the same temperature as the discharges. A Tenney Environmental T6S temperature chamber was used and the temperature accuracy within the chamber was determined to be within ±1 °C of the setpoint.

Electrochemical impedance spectroscopy (EIS) studies were also performed over a frequency range of 100 kHz to 2 mHz using a PAR 273A potentiostat coupled with a Solartron 1260 Impedance Analyzer. A 10-mV perturbation was used in all EIS studies.

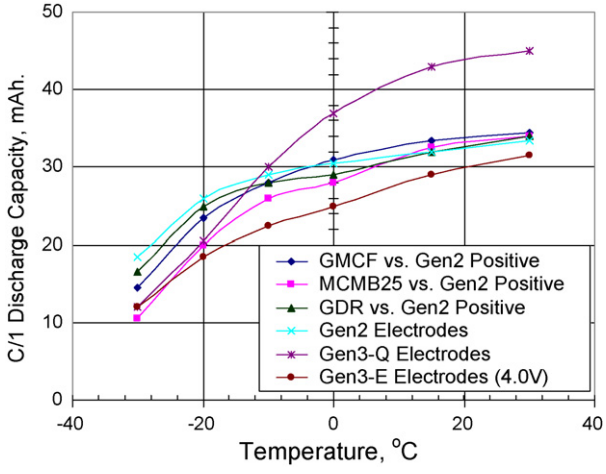

Fig. 2. Comparison of C/1 discharge capacity for electrodes used in this study. Cutoff voltage was 4.1 V for all cells except the Gen3-E cell (4.0 V).

3. Results and discussion

3.1. Capacity and impedance

The overall capacity results were generally similar for each cell system, especially for the cells that used the Gen2 positive electrodes. Constant voltage charging improved the capacity utilization, but the C/1 capacity at −30 °C was still roughly half of its 30 °C value (Fig. 2), whereas, with constant current charging, the C/1 capacity was less than a third of its value at 30 °C. The Gen3 electrodes were made to different specifications than the Gen2 electrodes; a higher negative to positive capacity ratio was used, and the Quallion electrodes were made with a higher loading density. Additionally, a lower cutoff voltage of 4.0 V was used for the Enerland electrode data shown in this work.

The area specific impedance (ASI) was calculated for the 10-s discharge and charge pulses that occur at 10% depth of discharge increments during the HPPC test. Normally, this is only done for the full cell, but with the inclusion of an interior micro-reference electrode, the ASI contribution from each electrode can be determined directly. These results are shown in Fig. 3 for the Gen2 cell system evaluated at 3.8 V as a function of temperature. The most significant observation from this data is that the negative and positive electrodes contribute nearly equally to the impedance rise at low temperature. The next significant observation is that the impedance of both electrodes increased significantly below 0 °C. This evidence suggests that two Arrhenius regions exist over this wide temperature range. The HPPC 10-s charge ASI behaved in a very similar manner, which suggests that the impedance rise affects the oxidation and reduction processes nearly symmetrically.

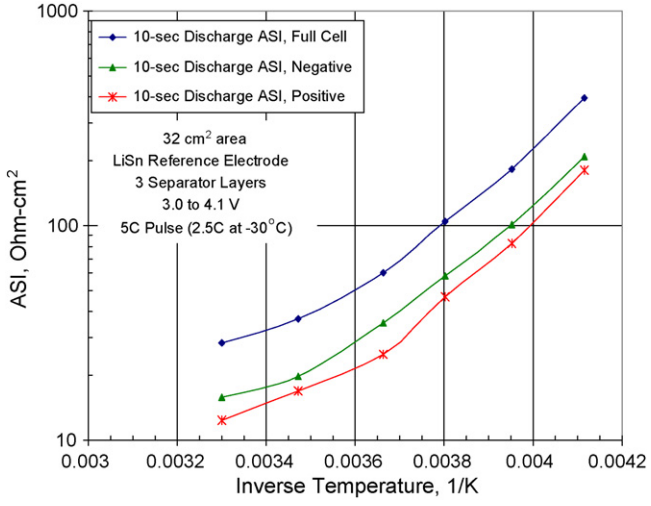

Fig. 3. HPPC 10-s discharge pulse ASI for full cell, negative electrode, and positive electrode from HPPC test evaluated at 3.8 V in a Gen2 cell. Cells with other electrodes had similar results.

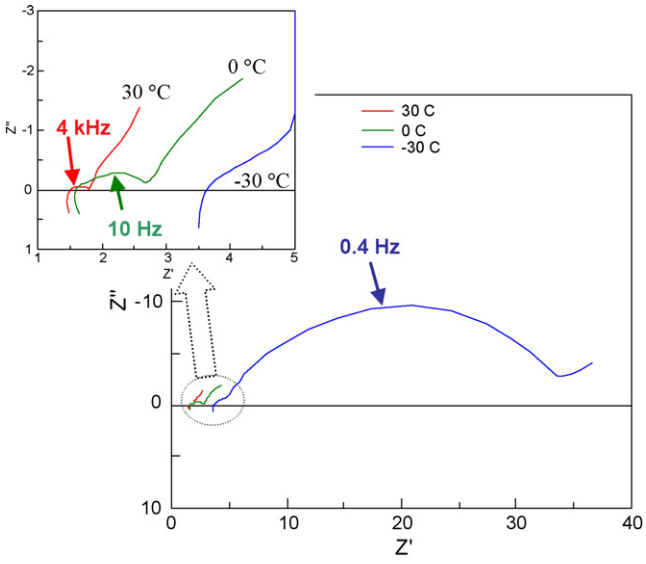

Fig. 4. Electrochemical Impedance Spectroscopy (EIS) results for Gen2 full cell at 30, 0, and −30 °C evaluated at 3.7 V. Units are in Ω.

These findings were further explored with EIS studies of this same cell. Here again, the value of the interior Li_ySn micro-reference electrode proved most useful. A smooth, "well-behaved" data set was obtained for each electrode as well as for the complete cell. These data are shown in Fig. 4, where the imaginary component of the impedance is plotted against the real component for temperatures of 30 °C, 0 °C, and −30 °C. The characteristic frequency is indicated for each of these curves. As with the HPPC data above, the most significant observation is the large impedance rise that occurs from 0 °C to −30 °C. This large impedance rise is clearly not due solely to a decreasing electrolyte conductivity, which would be evident at the high frequency intercept. It can be seen from the inset in this figure that the high frequency component of the real impedance increased by approximately 2 Ω when the temperature was lowered from 30 °C to −30 °C. Whereas, the mid-frequency component increased by nearly 33 Ω over the same temperature change. Similar findings were obtained by Fan [12] in 18,650-sized cells. The characteristic frequency was also observed to decrease by four orders of magnitude from 30 °C to −30 °C. This finding is being explored further.

Fig. 5 is a plot of the real and imaginary impedance for the Gen2 full cell with the contributions from the positive electrode and negative electrode obtained via the interior Li_ySn micro-RE at −30 °C. This also confirms the finding from Fig. 3 that the large impedance rise at low temperature is due to nearly equal contributions from the positive and negative electrodes. As a side note, similar experiments were tried using a lithium ingot in a region exterior to the electrode area with mixed results. While the general trends were the same as with the interior Li_ySn micro-RE, the EIS data curves occasionally exhibited loops and were highly dependent on the relative alignment of the positive and negative electrodes. A more complete discussion of the merits and limitations of interior and exterior reference electrodes can be found in the work of Dees et al. [9].

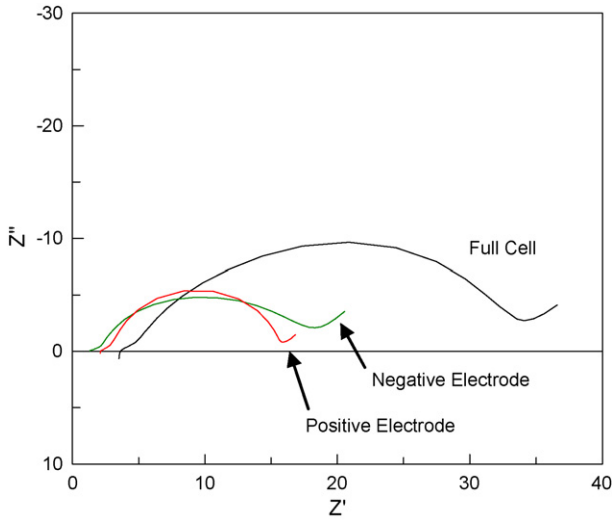

Fig. 5. EIS results for: Gen2 full cell; negative to Li_ySn RE; and positive to Li_ySn RE, at −30 °C evaluated at 3.7 V.

Other combinations of electrode materials were investigated to assess their low-temperature impedance response. A compilation of this full-cell HPPC ASI data is presented in Fig. 6. It is readily apparent that all of these cell systems have very similar performance over this wide temperature range. Two Arrhenius regions appear to exist with a crossover around 0 °C. Lines were added to Fig. 6 to aid in this visualization. This was also observed for other carbonate-based electrolytes systems and will be discussed in future work.

Although for brevity it is not shown here, the large impedance rise below 0 °C was observed to be due to nearly equal contributions from the positive and negative electrodes for all of these cell systems. This indicates that a mechanism that is more dominant than lithium diffusion in the active material is limiting the capacity and power at low temperature. It appears that the choice of active material does not have a significant effect on

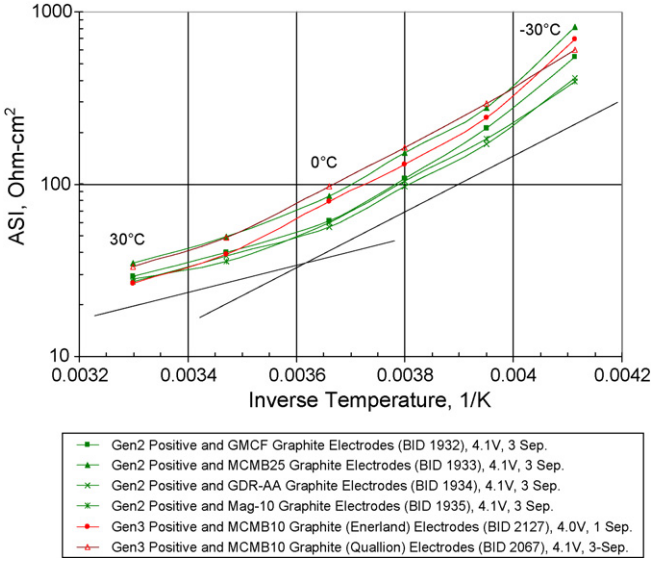

Fig. 6. Full-cell HPPC 10-s discharge pulse ASI evaluated at 3.8 V for cells used in this study. Cutoff voltage and number of separators indicated in legend.

the low-temperature performance. The EIS responses were also very similar to the response shown in Figs. 4 and 5. The bulk of the impedance rise at low temperature occurs in the mid-frequency region. Processes that take place in this frequency region are generally associated with interfacial effects. One can surmise from the observations made in this work that a power-limiting mechanism exists at the electrode-electrolyte interface that is relatively independent of the active material chemistry and dominates below 0 °C.

It is a daunting challenge to investigate the active material-electrolyte interface by any direct method in a full cell at low temperature. Dimensions of interest are nanoscale within composite electrodes that are only separated by 25 μm. The observation that the low temperature problem is relatively independent of active material implies that this problem is also independent of the solid electrolyte interface (SEI) since each active material has its own unique SEI layer. The commonality of the problem for all lithium-ion cell technologies suggests that it is associated with a fundamental phenomenon common to all lithium-ion electrodes, such as the kinetics of moving lithium ions across the electrochemical double layer to the active material surface. If the problem lies within the SEI at the active material interface, then additives to the cell chemistry with the design of changing the SEI, which have proven successful in stabilizing and/or reducing impedance, may not significantly impact the low temperature performance. Solutions to this problem must lie in affecting the properties that have a direct impact on the kinetics of the electrochemical reaction. One interesting phenomenon associated with the kinetics is the lithium solvation-desolvation process. Keeping in mind that the ASI is similar for both oxidation and reduction for all electrodes studied, further suggests the problem may be inherent to carbonate-based solvents.

3.2. Surface area considerations

Subtle variations in the data shown in Fig. 6 do exist and were explored further. One possible factor responsible for these variations, aside from active material, is the influence of surface area. The ASI of cells based on Gen3 positive material were generally higher than cells based on Gen2 positive material. The BET surface area of the Gen2 positive material is nearly twice that of the Gen3 positive material (Table 1).

A more direct comparison is available for the negative electrodes versus Gen2 positive. These data are presented in Fig. 7 in a non-log plot to highlight the impedance differences at low temperature. The HPPC ASI of the MCMB-25 is the highest, followed by the GMCF fiber, and then a tie between the GDR and the MAG-10 graphite. This inversely correlates well with the surface areas listed in Table 1 with the exception of the GDR and MAG-10. One would expect the MAG-10 to have the lowest ASI for this data set based on its high surface area. This anomaly could be due to the difference in particle morphology and/or surface treatment and may suggest that graphite materials with surface areas greater than ~3 m^2/g are preferred for high-power applications. Keep in mind that this simple analysis is based on BET surface area, whereas,

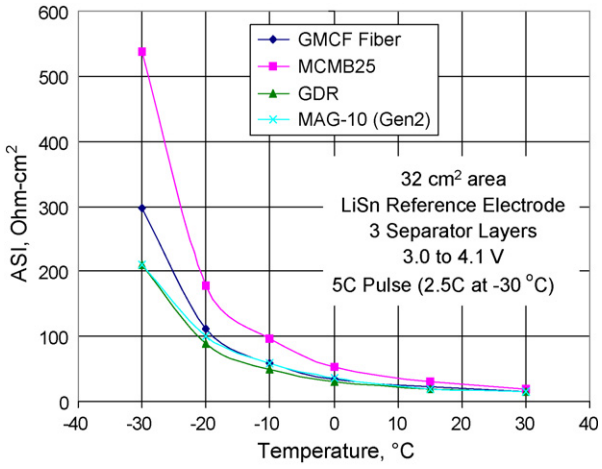

Fig. 7. Comparison of HPPC 10-s discharge pulse ASI for several graphite electrodes used in this study vs. Gen2 positive. Data were obtained with the use of a Li_ySn reference electrode in each full cell.

the parameter of real interest is the electrochemically active area.

Further evidence of the effect of surface area may be provided by ongoing research involving nano-sized particles of $Li_4Ti_5O_{12}$ for high-power batteries. This material was made at Argonne with a BET surface area of 2 m^2/g, which is considered to be quite high for a metal oxide material. The HPPC ASI of this electrode in a cell that incorporated a Li_ySn micro-RE is shown in Fig. 8. The HPPC ASI for the Gen2 positive and negative electrodes are included for comparison. The ASI for the titanium oxide is nearly constant above 0 °C and lower than either of the Gen2 electrodes. However, its ASI still increases significantly below 0 °C. The slope of the impedance rise is close to that of the Gen2 electrodes. This suggests that having a high surface area material will provide a lower ASI over a wider temperature range, but it still does not solve the poor low temperature performance problem.

All evidence suggests that the high ASI at low temperature is due to an electrode-electrolyte interface effect. Naturally then,

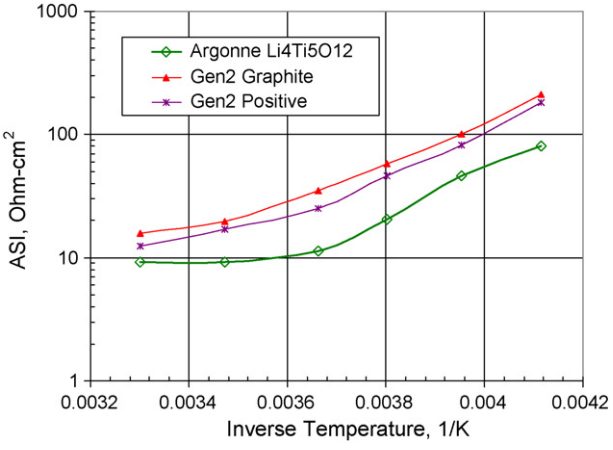

Fig. 8. HPPC 10-s discharge pulse ASI for Argonne's $Li_4Ti_5O_{12}$ compared to the Gen2 negative and positive electrodes. Data were obtained with the use of a Li_ySn reference electrode in each full cell.

increasing the surface area will help alleviate this problem, but not solve it. The effect of surface area will be explored more rigorously in the near future. Samples were obtained from graphite vendors that have variations in surface area without changes in particle morphology. This should provide a direct correlation between surface area and ASI at low temperature.

3.3. Lithium plating

Not only is the power of lithium-ion batteries severely limited at −30 °C, the concern also exists that lithium metal could plate on the negative electrode during regen (charge) pulses. Lithium plating on the negative electrode creates serious limitations on the cycle life of lithium ion batteries [13–14]. This deposited lithium reacts quickly with the surrounding electrolyte in an attempt to form a passivation layer (SEI). Unfortunately, this lithium consumption occurs on each cold charge pulse, resulting in a steady capacity loss.

The impact that graphite/carbon morphology has on susceptibility to lithium plating at low temperature was assessed using the *in situ* Li_ySn micro-RE. An additional reference electrode was added to some of these full cells that consisted of a small lithium ingot in a region exterior of the cell electrodes. In this manner the true potential of the Li_ySn reference electrode could be measured versus the electrochemically fixed lithium potential (Li_ySn has several voltage plateaus, see e.g. [15]).

HPPC tests were performed on each of the graphite electrodes versus the Gen2 or Gen3 positive electrodes with reference electrodes down to −30 °C. A widened cell voltage window of 1.5–4.6 V was used during the HPPC pulse segments to guarantee that the pulses were not terminated before the full 10-s duration was reached.

The potential of the Gen2 graphite electrode versus the lithium reference potential is plotted in Fig. 9. It is readily apparent that the graphite potential does dip below lithium potentials during charge pulses with the cell voltage window expanded to 4.6 V. (The cell voltage is listed below each charge pulse.) If the cell voltage is limited to 4.1 V, the potential for all of the charge pulses was above lithium potential. However, the graphite

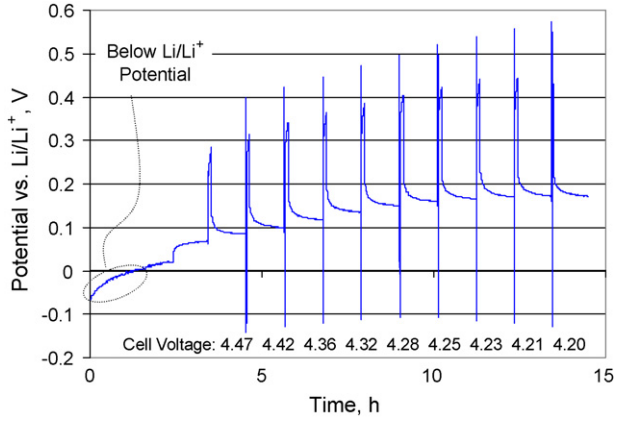

Fig. 9. Potential of the Gen2 graphite electrode vs. a lithium reference electrode during a HPPC test at −30 °C. Cathode was a Gen2 positive electrode.

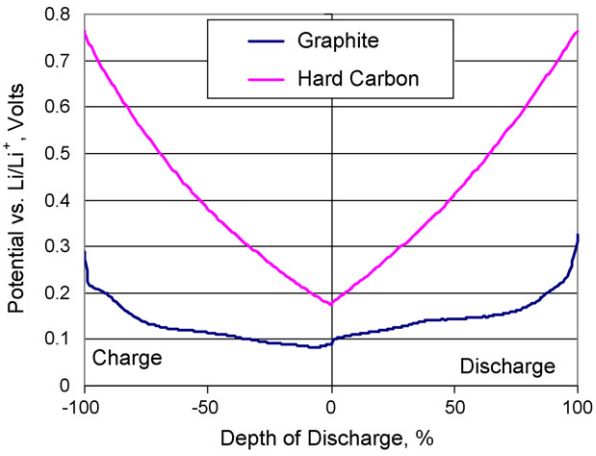

Fig. 10. Potential of graphite and hard carbon electrodes vs. Gen2 positive during cycling at C/2 rate at 30 °C (using dual reference electrodes).

potential remained below lithium potential during a portion of the constant voltage charge, as indicated in Fig. 9.

In general, it was found that below −20 °C the potential of all of the graphite negative electrodes used in this study dipped below lithium potentials not only during charge pulses but also under normal charging if the cell cutoff voltage was not reduced from its room-temperature value. This suggests that it is necessary to lower the cell cutoff voltage on low-temperature charges to a value less than 4.0 V. Another possible method of avoiding lithium plating is to oversize the negative electrode capacity relative to the positive electrode. However, this latter method may result in unacceptably high irreversible capacity loss during formation cycling.

A similar cell was built with hard carbon as the negative electrode versus a Gen2 positive electrode in Gen2 electrolyte. At no point in the charging process or the HPPC pulse charges did the hard carbon electrode potential go below lithium potential even though the cell voltage pulsed up to 4.4 V. This is because the hard carbon operates at potentials 200–800 mV above lithium potential, whereas, graphite has a long voltage plateau only 100 mV above lithium potential (Fig. 10).

It should be noted that no direct evidence of actual lithium metal was observed in these experiments. Within a few hundred milliseconds after the charge pulse, the potential of the negative electrode has easily relaxed to a potential above lithium potential. This indicates that the lithium does not exist as a metal plating, but rather, is consumed immediately in an attempt to form a passivation layer (SEI layer), or at the very least, does not have a firm electrical contact with the graphite matrix [16].

4. Conclusions

The most surprising finding from this work was that the impedance rise at low temperature was not significantly impacted by the choice of active material. The main rise in impedance occurs in the mid-frequency range. Processes that occur in this frequency range are generally interfacial in nature. This means that the responsible phenomenon is independent of the active material and is most likely an electrolyte-interface

effect. It should be noted that materials with high surface areas do appear to help the power performance at low temperature, but this is only part of the solution. Cells based on hard carbon and $Li_4Ti_5O_{12}$ as the negative electrode were much less likely to deposit lithium because they operate at potentials well above lithium potential. Efforts are now underway to investigate the influence of electrolyte properties such as composition, viscosity, density, dielectric strength, and wettability at low temperature.

Acknowledgments

Research funded by U.S. Department of Energy, FreedomCAR and Vehicle Technologies Program. The authors thank Tien Duong and David Howell of the FreedomCAR and Vehicle Technologies Program for their support. The authors also thank Ilias Belharouak, Jun Liu, and Sara Busking for their assistance.

References

[1] "FreedomCAR Battery Test Manual For Power-Assist Hybrid Electric Vehicles," DOE/ID-11069, available at http://www.uscar.org (2003).
[2] M.S. Ding, K. Xu, S.S. Zhang, K. Amine, G.L. Henriksen, T.R. Jow, J. Electrochem. Soc. 148 (2001) A1196.
[3] M.S. Ding, T.R. Jow, J. Electrochem. Soc. 150 (2003) A620.
[4] M.S. Ding, T.R. Jow, J. Electrochem. Soc. 151 (2004) A2007.
[5] L.F. Xiao, Y.L. Cao, X.P. Ai, H.X. Yang, Electrochim. Acta 49 (2004) 4857.
[6] M.C. Smart, B.V. Ratnakumar, S. Surampudi, J. Electrochem. Soc. 146 (1999) 4866.
[7] B.V. Ratnakumar, M.C. Smart, S. Surampudi, J. Power Sources 97–98 (2001) 137.
[8] M.C. Smart, B.V. Ratnakumar, L.D. Whitcanack, K.B. Chin, S. Surampudi, H. Croft, D. Tice, R. Staniewicz, J. Power Sources 119–121 (2003) 349.
[9] D.W. Dees, A.N. Jansen, D.P. Abraham, J. Power Sources. 174 (2007) 1001.
[10] C.S. Johnson, D.W. Dees, Proc. Electrochem. Soc. 94–4 (1994) 225.
[11] D.P. Abraham, S.D. Poppen, A.N. Jansen, J. Liu, D.W. Dees, Electrochim. Acta 49 (2004) 4763.
[12] J. Fan, J. Power Sources 117 (2003) 170.
[13] H.-P. Lin, D. Chua, M. Salomon, H.-C. Shiao, M. Hendrickson, E. Plichta, S. Slane, Electrochem. Solid State Lett. 4 (2001) A71.
[14] J. Fan, S. Tan, J. Electrochem. Soc. 153 (2006) A1081.
[15] I.A. Courtney, J.S. Tse, O. Mao, J. Hafner, J.R. Dahn, Phys. Rev. B 58 (1998) 15583.
[16] H. Yang, G.V. Zhuang, P.N. Ross, ECS Meeting Abstracts. (2006).